Title
Merging high-resolution satellite-based precipitation fields and point-scale rain gauge measurements-A case study in Chile

Journal
Journal of Geophysical Research, 122(10)

ISSN
0148-0227

Authors
Yang, Z
Hsu, K
Sorooshian, S
et al.

Publication Date
2017

DOI
10.1002/2016JD026177

AGU PUBLICATIONS

JGR

Journal of Geophysical Research: Atmospheres

RESEARCH ARTICLE
10.1002/2016JD026177

Key Points:
- A novel framework for merging satellite-based precipitation estimation and rain gauge observation
- Effective in producing high-resolution-precision precipitation data
- Supports for generalizing the mechanism for merging gauge and remotely sensed precipitation estimations worldwide

Correspondence to:
Z. Yang,
yangzw@craes.org.cn

Citation:
Yang, Z., K. Hsu, S. Sorooshian, X. Xu, D. Braithwaite, Y. Zhang, and K. M. J. Verbist (2017), Merging high-resolution satellite-based precipitation fields and point-scale rain gauge measurements—A case study in Chile, *J. Geophys. Res. Atmos.*, *122*, 5267–5284, doi:10.1002/2016JD026177.

Received 31 OCT 2016
Accepted 5 MAY 2017
Accepted article online 11 MAY 2017
Published online 27 MAY 2017

Merging high-resolution satellite-based precipitation fields and point-scale rain gauge measurements—A case study in Chile

Zhongwen Yang[1,2,3,4], Kuolin Hsu[4], Soroosh Sorooshian[4], Xinyi Xu[3], Dan Braithwaite[4], Yuan Zhang[1,2], and Koen M. J. Verbist[5,6]

[1]State Key Laboratory of Environmental Criteria and Risk Assessment, Chinese Research Academy of Environmental Sciences, Beijing, China, [2]Laboratory of Riverine Ecological Conservation and Technology, Chinese Research Academy of Environmental Sciences, Beijing, China, [3]College of Water Sciences, Key Laboratory of Water and Sediment Sciences of Ministry of Education, Beijing Normal University, Beijing, China, [4]Department of Civil and Environmental Engineering, University of California, Irvine, California, USA, [5]Hydrological Systems and Water Scarcity Section, UNESCO-IHP, Santiago, Chile, [6]International Centre for Eremology, Department of Soil Management, Ghent University, Ghent, Belgium

Abstract With high spatial-temporal resolution, Satellite-based Precipitation Estimates (SPE) are becoming valuable alternative rainfall data for hydrologic and climatic studies but are subject to considerable uncertainty. Effective merging of SPE and ground-based gauge measurements may help to improve precipitation estimation in both better resolution and accuracy. In this study, a framework for merging satellite and gauge precipitation data is developed based on three steps, including SPE bias adjustment, gauge observation gridding, and data merging, with the objective to produce high-quality precipitation estimates. An inverse-root-mean-square-error weighting approach is proposed to combine the satellite and gauge estimates that are in advance adjusted and gridded, respectively. The model is applied and tested with the Precipitation Estimation from Remotely Sensed Information using Artificial Neural Networks-Cloud Classification System (PERSIANN-CCS) estimates (daily, 0.04° × 0.04°) over Chile, for the 6 year period of 2009–2014. Daily observations from about 90% of collected gauges over the study area are used for model calibration; the rest of the gauged data are regarded as ground "truth" for validation. Evaluation results indicate high effectiveness of the model in producing high-resolution-precision precipitation data. Compared to reference data, the merged data (daily) show correlation coefficients, probabilities of detection, root-mean-square errors, and absolute mean biases that were consistently improved from the original PERSIANN-CCS estimates. The cross-validation evidences that the framework is effective in providing high-quality estimates even over nongauged satellite pixels. The same method can be applied globally and is expected to produce precipitation products in near real time by integrating gauge observations with satellite estimates.

1. Introduction

Precipitation is a key process in the hydrological cycle. The quality of precipitation data is of high importance to hydrologists, as precipitation uncertainty is the most influential cause of uncertainty in hydrological simulation [*Moradkhani and Sorooshian*, 2008]. As such, it is significant to accurately quantify the precipitation rate for reliable hydrological applications.

Rain gauge measurements and satellite-based estimations are two precipitation data sources with different features. A rain gauge network directly measuring precipitation is capable of providing reliable observations with high accuracy. But the uncertainty of precipitation increases when the point-wise measurements are extended to areas where gauges are nonexistent [*Huff*, 1970]. This situation becomes even worse over mountainous or arid/semiarid regions with sparsely distributed gauges [*Chubb et al.*, 2016; *King et al.*, 2013; *Miao et al.*, 2015; *Tozer et al.*, 2012]. Therefore, Satellite-based Precipitation Estimates (SPE) are becoming a popular alternative for measuring precipitation, particularly over those gauge-sparse areas. It can provide high-resolution and global coverage SPE products based on remotely sensed information from geostationary Earth-orbiting (GEO) or/and low Earth-orbiting satellites [*Hong et al.*, 2004; *Hsu et al.*, 1997, 1999; *Huffman et al.*, 2010, 2007, 2014; *Joyce et al.*, 2004; *Kubota et al.*, 2007; *Mitchell et al.*, 2004; *Sorooshian et al.*, 2000]. Nevertheless, these SPE products are subject to considerable biases [*AghaKouchak et al.*, 2011; *Li et al.*, 2013;

Melo et al., 2015; *Miao et al.*, 2016b; *Satge et al.*, 2016; *Yang et al.*, 2016]. This limitation leads to relatively high uncertainties in hydrologic modeling [*Behrangi et al.*, 2014; *Bitew and Gebremichael*, 2011; *Gebregiorgis et al.*, 2012; *Thiemig et al.*, 2013; *Yang et al.*, 2017]. This has further motivated the use of uncertainty analysis models to investigate the bias characteristics of SPE [*Liu et al.*, 2015; *Sarachi et al.*, 2015; *Tian et al.*, 2009]. Based on these studies, it was recommended that merging SPE and gauged data might improve the resolution, accuracy, and coverage of precipitation estimations.

Since the late 1990s, researchers started to put efforts into combining satellite-gauge precipitation data. The early successful work was the Global Precipitation Climatology Project (GPCP), which constructed a relatively coarse-resolution (monthly, 2.5° × 2.5°) global precipitation data set [*Adler et al.*, 2003; *Huffman et al.*, 1997]. In the GPCP, a mean bias correction method and an inverse-error-variance weighting approach were employed to produce a merged analysis that benefited from both the spatial coverage of satellite estimates and the accuracy of ground observations. *Ashouri et al.* [2015] further incorporated the GPCP rainfall data into the Precipitation Estimation from Remotely Sensed Information using Artificial Neural Networks (PERSIANN) rainfall estimates, providing a useful data record for climatic studies (termed the PERSIANN-CDR) with higher resolution (daily, 0.25° × 0.25°) [*Ashouri et al.*, 2015].

Recent studies merging satellite and gauge data have focused on some high-resolution SPE products. *Vila et al.* [2009] combined the Real-time TRMM Multisatellite Precipitation Analysis (TMPA) daily estimates with gauge measurements using a bias correction scheme. *Li and Shao* [2010] employed a nonparametric kernel smoothing model to estimate the error field of TMPA estimates, resulting in bias-reduced satellite-gauge merged precipitation data. Notably, some studies tried to indirectly merge satellite and gauge estimations by considering an advance step for adjusting the systematic biases in satellite data. *Xie and Xiong* [2011] conducted a conceptual merging framework that included a SPE bias correction step and a satellite-gauge data combination step. In the SPE bias correction step, systematic biases of satellite precipitation retrievals were effectively reduced. Systematic bias correction was also recommended by *De and Terra* [2012] in satellite-gauge data merging.

In our previous work [*Yang et al.*, 2016], a probability-based bias adjustment approach for SPE (termed the quantile mapping technique-Gaussian weighting scheme (QM-GW)) was developed and tested over Chile, using the Precipitation Estimation from Remotely Sensed Information using Artificial Neural Networks-Cloud Classification System (PERSIANN-CCS) [*Hong et al.*, 2004]. This approach was shown to have high effectiveness in adjusting systematic biases of SPE even into the future, but it was not effective in addressing random errors. A recent study has compared the QM-GW-adjusted PERSIANN-CCS data with multiple satellite precipitation products over Chile [*Zambrano-Bigiarini et al.*, 2017]. This study shows that our bias-adjusted PERSIANN-CCS (Adj-CCS) estimates are worse in representing observed rainfall than those products, including the PGFv3 [*Chaney et al.*, 2014; *Peng et al.*, 2016], CHIRPSv2 [*Funk et al.*, 2015], TMPA 3B42v7 [*Huffman et al.*, 2010], and MSWEPv1.1 [*Beck et al.*, 2016]. It is worth mentioning that the Adj-CCS product was generated based on 5 year historical data trained probability matching (QM-GW approach) with no additional gauge data included. However, all of the other four data sets are merged products including both satellite and gauge observations over the same time period (e.g., for each specific month). That means while the QM-GW approach is advanced in adjusting SPE into the future compared to those data merging algorithms, it neglected the contribution of simultaneous gauge observations to adjusted precipitation results, which is the main reason for the poorer performance of Adj-CCS estimates over Chile. Building on those results, in order to gain better precipitation products, we expect to construct a robust framework that merges the QM-GW-adjusted satellite estimates with gauge observations at the end of each day when real-time daily data are made available.

In this study, a framework for merging high-resolution satellite precipitation estimation and point-wise gauge observation is developed to provide high-quality precipitation data supporting hydrological and climatic applications. The model blends satellite and gauge data in three procedures: (1) SPE bias adjustment, (2) gauge measurement gridding, and (3) data merging. To test the model, a case study is demonstrated in Chile using daily retrievals from the PERSIANN-CCS [*Hong et al.*, 2004] and collocated gauge data for the period of 2009–2014. The methodology and case study being presented in this work are intended to generalize the mechanism for merging gauge and remote-sensing precipitation data in other regions of the world, if the minimum amount of in situ data is available. The rest of this paper is organized as follows: section 2 presents

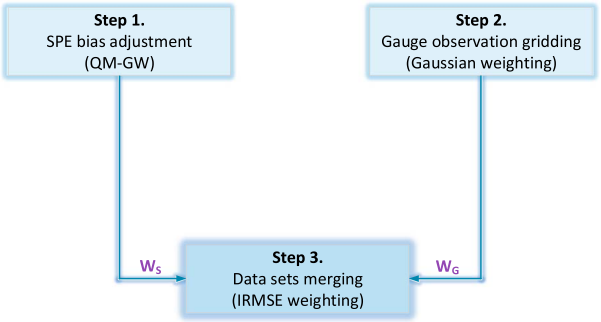

Figure 1. Framework for merging satellite and gauge precipitation estimates.

the methodology, section 3 describes the case study, section 4 presents the evaluation results, and the conclusions and future prospect are given in section 5.

2. Methodology

From Figure 1, three steps for the satellite-gauge data merging framework are presented. In the first step the systematic biases in satellite precipitation retrievals are removed using the QM-GW approach developed by *Yang et al.* [2016]. In the second step, observations from gauge stations are gridded over satellite pixels (at the same resolution of satellite data) based on a Gaussian weighting scheme. Finally, an inverse-root-mean-square-error (IRMSE) weighting approach is employed to blend the bias-adjusted and gridded data sets. Details of the methods for the three steps are described in the following sections.

2.1. SPE Bias Adjustment

In the bias adjustment procedure, the QM-GW approach was constructed based on a quantile mapping (QM) technique and a Gaussian weighting interpolation scheme [*Yang et al.*, 2016]. The QM is a probability-based technique that corrects the systematic biases in satellite estimations based on a cumulative distribution function (CDF) transformation using CDFs calculated with historical precipitation data from gauge stations and collocated satellite pixels [*De and Terra*, 2012; *Miao et al.*, 2016a; *Themessl et al.*, 2012]. Specifically, the QM-GW approach calculates seasonal nonparametric CDF pairs (from satellite and gauge data) at each 1° × 1° grid box area divided in advance [*Yang et al.*, 2016]. In doing so, we assume that the gauges or satellite pixels within each 1° × 1° grid box share the same CDF for precipitation, which is reasonable because the probability distributions for multiple years of precipitation events generally exhibit spatial homogeneity in a local area. Thus, the CDF pairs over a specific grid box are calculated using mixed precipitation estimates from the included gauges and collocated satellite pixels. For those 1° × 1° grid boxes with no gauge stations, the concurrent gauge and satellite estimates from nearby 1° × 1° grid boxes are collected to estimate the CDFs for that grid box. Based on those CDFs, a satellite precipitation estimation over a given pixel is primarily corrected using the CDF pairs from four neighboring 1° × 1° grid boxes, resulting in four bias-corrected estimations. In addition, the Gaussian weighting interpolation scheme is utilized to estimate the final adjusted precipitation rate by interpolating those bias-corrected estimations using distance-based weighting with a Gaussian function. Details of the QM-GW approach can be found in *Yang et al.* [2016].

2.2. Gauge Observation Gridding

In previous studies, point-wise gauge observations were directly merged with satellite data [*Li and Shao*, 2010; *Vila et al.*, 2009; *Xie and Xiong*, 2011]. However, in this study, a separate step is used to grid the gauge data in the same spatial resolution as satellite retrievals. The gridded gauge observation (Gri-GO) at satellite pixel *i* is estimated based on a Gaussian weighting function to the neighboring gauges that are included within four nearby gauged 1° × 1° grid boxes (see equations (1)–(3)). The four nearby grid boxes are chosen using the shortest distances (top four) from pixel *i* to the centers of those gauged 1° × 1° grid boxes. By doing so, generating a localized interpolation is aided by ignoring unnecessary gauges that are far away from pixel *i* which reduces the computation load, considering that a large number of rain gauges may exist over a given study area.

$$R_{Gi}^{\mathrm{gri}} = \sum_{j=1}^{n} w_{ij} r_{Gj} \tag{1}$$

$$w_{ij} = \exp\left(-\left(\overline{d}_{ij}/C\right)^2\right) / \sum_{j=1}^{n} \exp\left(-\left(\overline{d}_{ij}/C\right)^2\right) \tag{2}$$

$$\overline{d}_{ij} = d_{ij}/D \tag{3}$$

where R_{Gi}^{gri} is gridded gauge measurement for pixel *i*; r_{Gj} is gauge observation at station *j*; *n* is the number of

gauge stations included in the four neighboring gauged grid boxes (divided in the SPE bias adjustment step) of pixel i; w_{ij} is the weight assigned for gauge j; d_{ij} and $\overline{d}_{ij}$ are the actual and normalized straight-line distances, respectively, between pixel i and gauge j; D is a constant that equals the maximum straight-line distance within the four neighboring grid box area; and C is a shape parameter for the Gaussian function.

It is worth mentioning that this gauge data gridding approach leads to additional uncertainties in gridded observations when point-scale data are interpolated over high spatial resolution fields. Generally, gridded gauge precipitation data tend to underestimate extreme wet events and overestimate the frequency and amount of very low rainfall events, implying that gridded estimates might not accurately represent "real" spatial and temporal variabilities of precipitation [*King et al.*, 2013; *Tozer et al.*, 2012]. In this case, it is of importance to quantify the uncertainty of the gridded gauge measurements (R_{Gi}^{gri}) as they are used for satellite-gauge data merging.

2.3. Data Set Merging

According to *Yang et al.* [2016] and the gauge data gridding approach presented above, biases remain in both the bias-adjusted SPE (using QM-GW approach) and the Gri-GO (in satellite resolution). In this context, the IRMSE weighting approach is developed to merge the bias-adjusted and gridded precipitation data sets based principally on the root-mean-square errors (RMSEs) quantifying uncertainties of the data sets, as detailed below.

When the bias-adjusted satellite estimates and gridded gauge observations are ready, merged satellite-gauge precipitation (Mer-SG) is calculated using equations (4)–(6):

$$R_i^{\mathrm{mer}} = W_{Si} R_{Si}^{\mathrm{adj}} + W_{Gi} R_{Gi}^{\mathrm{gri}} \tag{4}$$

$$W_{Si} = \left(\frac{1}{\mathrm{RMSE}_{Si}}\right) \Big/ \left(\frac{1}{\mathrm{RMSE}_{Si}} + \frac{1}{\mathrm{RMSE}_{Gi}}\right) \tag{5}$$

$$W_{Gi} = \left(\frac{1}{\mathrm{RMSE}_{Gi}}\right) \Big/ \left(\frac{1}{\mathrm{RMSE}_{Si}} + \frac{1}{\mathrm{RMSE}_{Gi}}\right) \tag{6}$$

where R_i^{mer} is the merged precipitation rate for pixel i; R_{Si}^{adj} is the bias-adjusted SPE for pixel i; W_{Si} and W_{Gi} are weights calculated seasonally for the bias-adjusted satellite and gridded gauge estimates, respectively; RMSE_{Si} and RMSE_{Gi} are RMSEs estimated for the two data sets over pixel i, respectively, by equations (7) and (8):

$$\mathrm{RMSE}_{Si} = \frac{1}{N}\sum_{j=1}^{N} \sqrt{\frac{1}{m}\sum_{k=1}^{m}\left(R_{Sjk}^{\mathrm{adj}} - r_{Gjk}\right)^2} \tag{7}$$

$$\mathrm{RMSE}_{Gi} = f(\mathrm{DMIN}_i) \tag{8}$$

where R_{Sjk}^{adj} is the k th bias-adjusted satellite precipitation rate over the pixel that includes gauge j; , r_{Gjk} is gauge observation from gauge j; , N is the total number of gauge stations and m represents the total number of precipitation rates from gauge j; , and $f(\mathrm{DMIN}_i)$ is the outcome from an increasing function that depicts the RMSE_{Gi} increase when the distance between pixel i and its nearest gauge station (DMIN_i) grows.

According to equation (7), the error term RMSE_{Si} is assumed to be constant over the entire study area and estimated directly using the observations and adjusted estimates from rain gauges and collocated satellite pixels, respectively. The error function $f(\mathrm{DMIN})$ in equation (8) can be fitted to the calculated samples of RMSE for gridded observation at every gauge ($\mathrm{RMSE}^{\mathrm{gri}}$) and corresponding minimal distance from each gauge to the others (D_{min}). In this case, a cross-validation strategy is applied to obtain the $\mathrm{RMSE}^{\mathrm{gri}}$ samples:

$$\mathrm{RMSE}_j^{\mathrm{gri}} = \sqrt{\frac{1}{m}\sum_{k=1}^{m}\left(R_{G-jk}^{\mathrm{gri}} - r_{Gjk}\right)^2} \tag{9}$$

where $\mathrm{RMSE}_j^{\mathrm{gri}}$ represents the $\mathrm{RMSE}^{\mathrm{gri}}$ at gauge station j; and R_{G-jk}^{gri} is gridded gauge observation over gauge

station *j* by discarding self-point observed data, which uses the same Gaussian weighting scheme as step 2 (Figure 1) with fixed parameters.

3. Case Study

This section describes a case study in Chile (study area description can be found in *Yang et al.* [2016]) for testing the data merging framework. Data sources, model calibration, and evaluation strategies of the case study are described as follows.

3.1. Data Sources

This study is conducted based on the same precipitation data series (daily) collected by *Yang et al.* [2016]. These data include the original PERSIANN-CCS precipitation retrievals (Ori-CCS, 0.04° × 0.04°) and gauge observations over Chile for the 6 year period of 2009–2014. Detailed information about the two data sources was presented in *Yang et al.* [2016]. It is worth mentioning that the study area is limited to the latitude extent from 17°S to 46°S (Figure 2). This is due to insufficient samples from GEO sensors over the remaining part of Chile (46°S–56°S) for PERSIANN-CCS precipitation estimation [*Yang et al.*, 2016]. In this case, a total of 456 gauges were collected over the study area, the same as in *Yang et al.* [2016].

Notably, as shown in *Yang et al.* [2016] the Adj-CCS (for 2009–2014) over Chile had been already generated using the QM-GW approach based on the same data sources. As such, we take these Adj-CCS estimates as the outcomes from the SPE bias adjustment step in this study (see Figure 3).

3.2. Model Calibration

The flowchart for calibrating and validating the model is shown in Figure 3. As the QM-GW bias adjustment approach has already been validated by *Yang et al.* [2016], this case study focuses on steps 2 and 3 in order to identify if the extended framework can further improve precipitation estimation via satellite-gauge data merging. Therefore, for model calibration purposes, daily precipitation measurements from 414 gauges (about 90% of the gauge data; see Figure 4a) are gridded in satellite pixels (0.04° × 0.04°) and then merged with the Adj-CCS estimates for 2009–2014 (Figure 3). Forty-two rain gauges covering the extent of the study area were not included in the calibration process and were used to validate the effectiveness of the proposed merging procedure (Figure 4b). These validation gauges were selected randomly from the north, middle, and south of the study area within a minimum distance ($<$ 40 km) of at least one calibration gauge. The parameterization procedures for gauge data gridding (step 2) and data set merging (step 3) are described as follows.

3.2.1. Parameterization for Gauge Data Gridding

As presented in Figure 2, the study area (extending from 17°S to 46°S) is initially divided into 98 grid boxes (1° × 1°). For a given satellite pixel, the gridded precipitation estimate is calculated using the observations from the four nearby gauged 1° × 1° boxes (according to equations (1)–(3)). In doing so, the value of the shape parameter *C* needs to be determined in advance. In this study, the estimation for *C* is based on a correlation coefficient (CORR) analysis strategy described as follows:

First, a large number of CORRs are calculated for the observed precipitation time series from any two calibration gauges that are included in any four neighboring 1° × 1° boxes. Correspondingly, the normalized distance (ND) between each pair of calibration gauges is estimated by dividing the geographical distance with the same constant *D* used in the gauge data gridding step (see equation (3)). A CORR-ND relationship has been fitted to these samples of CORR and ND (Figure 5). It can be inferred from the fitted function curve that precipitation for a given pixel is less related to the obervations from farther located gauge stations, showing lower CORRs (ranging from 0 to 1). In this case, any gauge station with a CORR to a gridded pixel of less than a critical value, say *a*, ought to have limited contribution to the final gridded precipitation rate due to long distance. The limited contribution is represented by a small Gaussian function value according to the gridding approach (see equations (1)–(3)). Based on these inferences, two inequations can be constructed shown as equations (10) and (11):

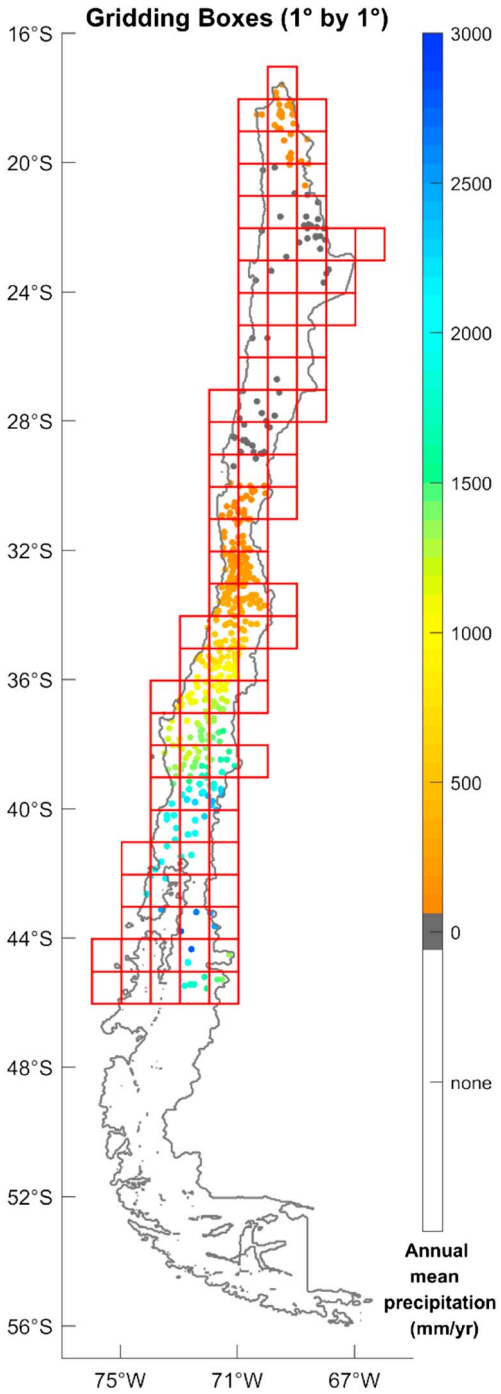

Figure 2. Grid boxes (1° × 1° red boxes) and 414 included calibration gauges over the study area.

$$\left(\frac{1}{\mathrm{ND}+1}\right)^{1.4155} < a \quad (10)$$

$$f(\mathrm{ND}) = \exp\left(-\frac{\mathrm{ND}^2}{C^2}\right) < b \quad (11)$$

where b is a critically small Gaussian function value.

In this case study, we determined the values of [a, b] as [0.5, 0.1]. This determination helps to effectively avoid interferences from those gauges with relatively low precipitation correlationships to specific gridded pixel estimation in the gauge data gridding procedure. This is because any gauge station that has a less than 0.5 CORR to gridded pixel will be assigned as a Gaussian function value of less than 0.1, presenting limited influence on gridding results. Based on the assignments, the resolutions of the equations (10) and (11) are $\mathrm{ND} > 0.6318$, $C < 0.4164$. Therefore, we finally determine the shape parameter, $C = 0.4$, for gridding the gauge observations during 2009–2014.

3.2.2. Fitting Seasonal Weighting Functions for Data Merging

According to the data merging approach, mean RMSE of the Adj-CCS data is estimated directly and separately for the four seasons with equation (7). The seasonal error function f(DMIN) has been fitted to the $\mathrm{RMSE}^{\mathrm{gri}} - D_{\mathrm{min}}$ samples calculated based on equation (9). The results are shown in Figure 6.

Based on the fitted weighting functions shown in Figure 6, the Gri-GO and Adj-CCS precipitation estimates can be blended together using equations (4)–(8). It can be inferred that the Gri-GO estimates for a pixel i that has a distance of less than about 40 km to its closest gauge will be given a higher weight than the collocated Adj-CCS data, when the two data sets are combined. However, the contribution of Adj-CCS to the Mer-SG estimation will increase as the distance between pixel i and its closest gauge increases.

3.3. Evaluation Strategy

The precipitation estimates (Ori-CCS, Adj-CCS, and Mer-SG) from model calibration are compared to show how the data merging framework improves precipitation estimation step by step, especially when the gridded gauge data are incorporated. The gridded gauge observations (Gri-GO, at 0.04° × 0.04° resolution)

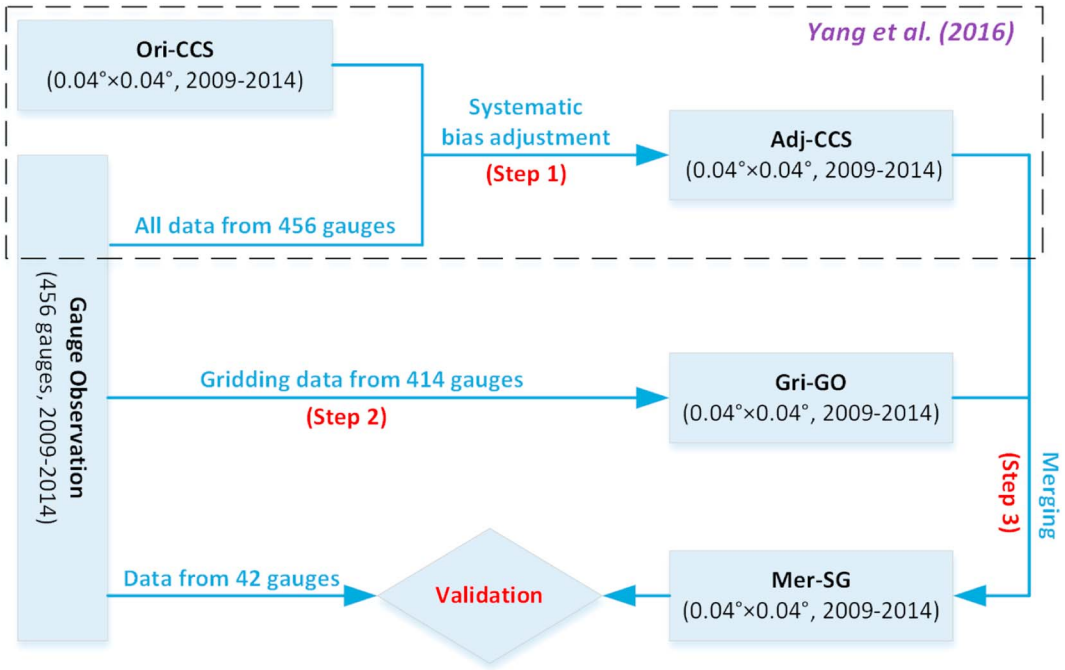

Figure 3. Flowchart for model calibration and validation using daily satellite and gauge precipitation retrievals over Chile.

are used as reference for the comparison. The Gri-GO is closer to the real precipitation field exhibiting much lower RMSEs than the Adj-CCS. This is as expected considering the high gauge density over the study area with an average distance between gauges calculated to be 15.76 km (Figure 4a). In the comparison process, the precipitation estimation is assessed with respect to its spatial pattern and temporal distribution, similar to the procedure applied in *Yang et al.* [2016]. The spatial pattern evaluation examines the spatial improvement of precipitation data, taking the study area as a whole. For the temporal scale assessment, three evaluation zones (see Figure 4a), with a 2° latitude extent representing low-, medium-, and high-precipitation regions, are selected, which follows *Yang et al.* [2016]. These zones are used to present the time series evaluations (both monthly and daily) for areal mean precipitation.

For validating the developed framework, the precipitation estimates are examined over those pixels where included gauges are not involved in the model calibration. Specifically, we use measurements from the validation gauges (Figure 4b) as precipitation "truth" to evaluate the performance of the precipitation estimation after applying the merging procedure. These validation gauges are classified into three groups, representing low-, middle-, and high-latitude regions, and the rainfall averages for each of the groups are evaluated.

The performances of the Ori-CCS, Adj-CCS, and Mer-SG estimates are indicated by three statistics: the CORR, the RMSE, and the mean bias (BIAS). The calculation of the statistics were done as described in *Yang et al.* [2016], with higher CORR and lower RMSE and absolute BIAS representing better performance of precipitation estimation. Furthermore, the probability of detection (POD), false alarm ratio (FAR), and Heidke skill score (HSS) are estimated for daily precipitation time series to view the hits and misses. The calculation of the three indicators follow *Hyvarinen* [2014] and *Su et al.* [2011].

4. Evaluation

4.1. Calibration Results

4.1.1. Climatological Pattern Comparison

Figure 7 compares the annual averages of Ori-CCS, Adj-CCS, and Mer-SG precipitation estimates for the period of 2009–2014. Compared to Gri-GO, Ori-CCS overestimated precipitation over northern Chile and underestimated in the south, and the Adj-CCS shows greatly improved spatial patterns of precipitation versus Ori-CCS due to systematic bias adjustment. After merging Gri-GO and Adj-CCS, the Mer-SG exhibits further improved spatial consistency with Gri-GO. The scatterplot comparisons over gauged pixels evidence these

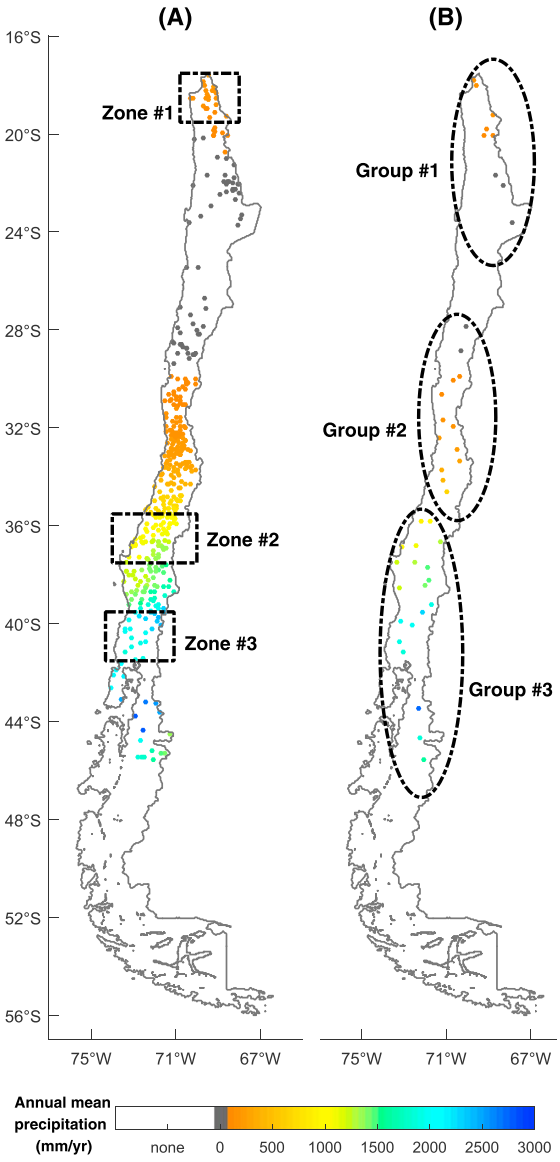

Figure 4. (a) Calibration gauges and locations of evaluation zones. (b) Validation gauges and three gauge groups classified.

changes as well (Figure 7), showing that the Mer-SG outperforms Ori-CCS and Adj-CCS, with the red dots distributed tightly around the 1:1 line. This is indicated by the very high CORR (~1.0), as well as the lowest RMSE (10.27 mm/yr) and absolute BIAS (1.52 mm/yr) values for the Mer-SG precipitation estimates.

Furthermore, the monthly spatial patterns of the different precipitation estimations are compared for January, April, July, and October. From Figure 8, the monthly precipitation averages for the four months during 2009–2014 exhibit similar results to those for the annual averages. Ori-CCS shows overestimated monthly average precipitation in northern Chile and underestimated in the south, resulting in low CORRs and high RMSEs as compared to the observations over collocated gauges. After systematic bias adjustment and data merging, these spatial disagreements have been significantly reduced (Figure 8). Both the Adj-CCS and Mer-SG show well-corrected spatial patterns for monthly precipitation averages compared to Gri-GO. In particular, Mer-SG exhibits the best performance. Due to blending satellite and gauge estimates, the RMSEs and absolute BIASs for Mer-SG monthly averages in gauged pixels decreased to around 1.0 and less than 0.4 mm/month, respectively. As expected, the CORRs for Mer-SG reached values as high as 1.0.

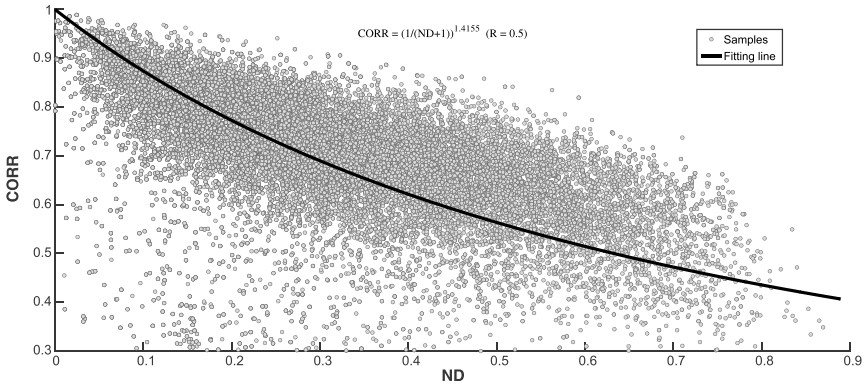

Figure 5. Fitted function curve (black line) for the CORR-ND relationship (corresponding formulation is shown on the top).

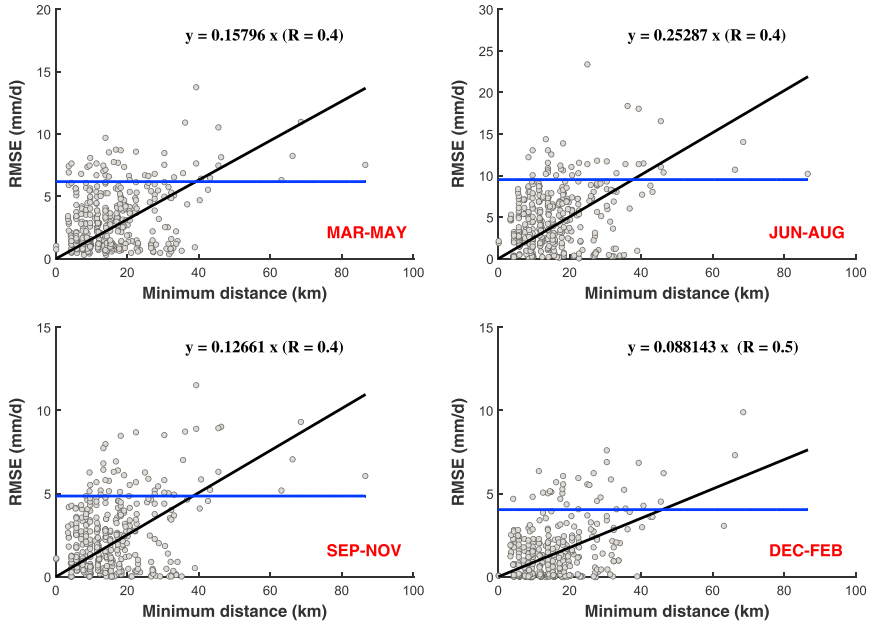

Figure 6. Seasonal RMSE-minimum distance relationships for the Gri-GO (black line) and Adj-CCS (blue line) estimates. The black lines are fitted to the samples (grey points) for four seasons, and corresponding formulations are presented on the top, respectively.

4.1.2. Time Series Comparison

4.1.2.1. Monthly

The monthly precipitation series are presented with plots of Gri-GO, Ori-CCS, Adj-CCS, and Mer-SG over zone nos. 1, 2, and 3 for 2009–2014, as presented in Figure 9. Compared to Gri-GO, consistent overestimations of monthly precipitation from Ori-CCS are seen over zone no. 1 and underestimations for zone nos. 2 and 3. These disagreements result in high RMSEs (over 52.74 mm/month) and absolute BIASs (exceeding 33.86 mm/month). After systematic bias adjustment, the Adj-CCS presents consistent improvement in monthly precipitation series, indicated by the largely reduced RMSEs and absolute BIASs by 51% and 92% on average, respectively (Figure 9). However, the Adj-CCS does not well capture precipitation for some specific months (e.g., August 2012), especially over the high precipitation zone nos. 2 and 3, resulting in relatively high RMSEs (over 50 mm/month) and no distinct improvement of the CORRs. Similar changes were found in *Yang et al.* [2016] as well.

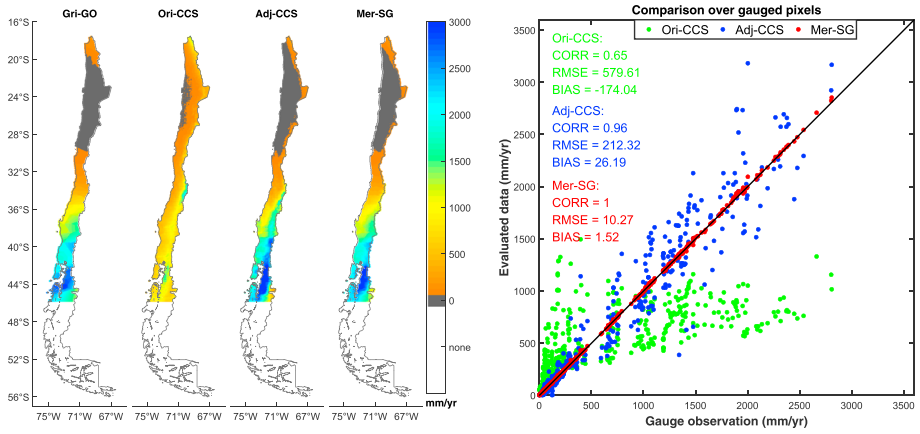

Figure 7. (left) Annual average precipitation of Gri-GO, Ori-CCS, Adj-CCS, and Mer-SG during 2009–2014 and the (right) corresponding comparison of Ori-CCS (black dots), Adj-CCS (blue dots), and Mer-SG (red dots) over gauged pixels.

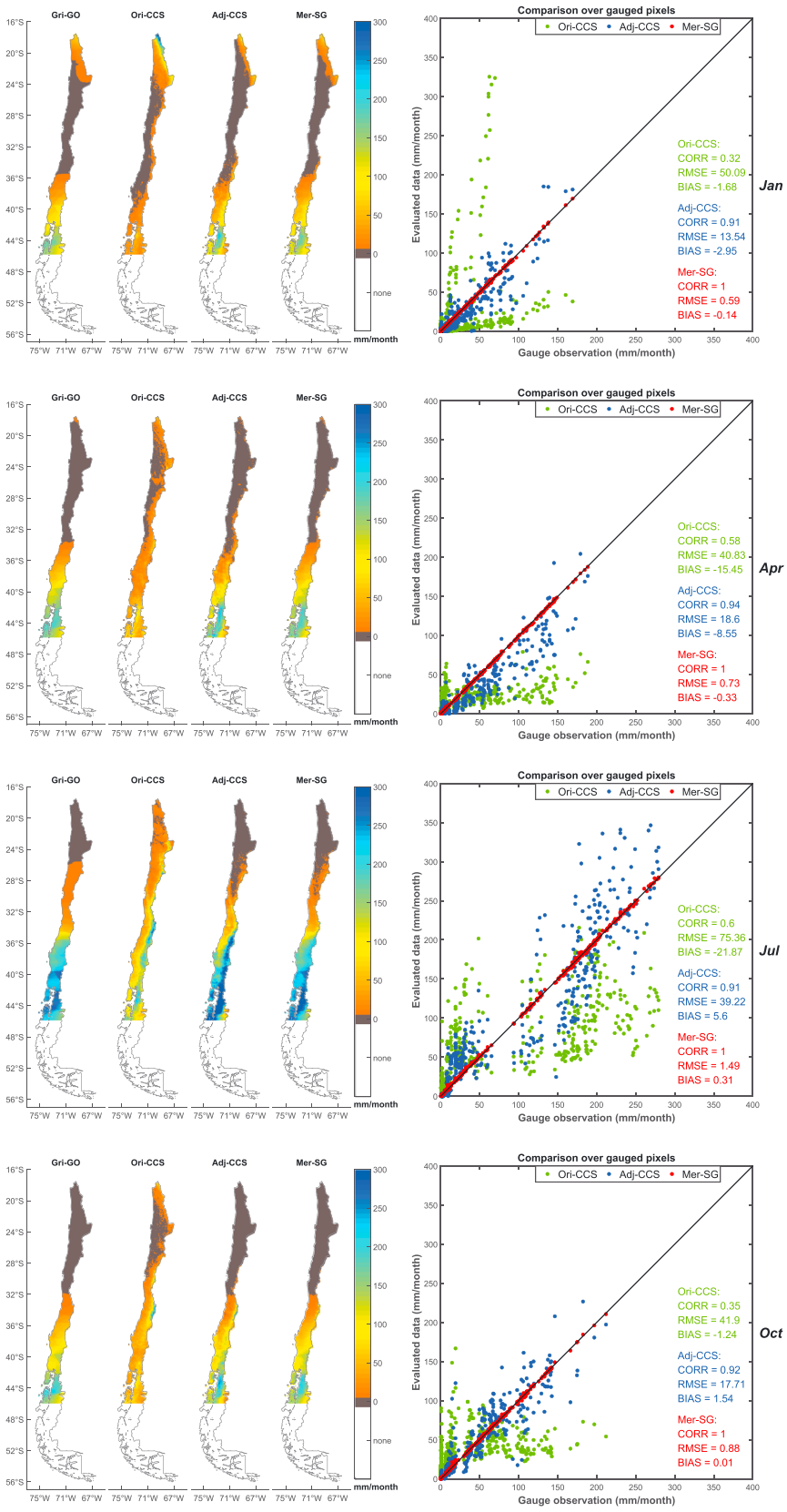

Figure 8. As in Figure 7 but for monthly average results for January, April, July, and October (from top to bottom), respectively.

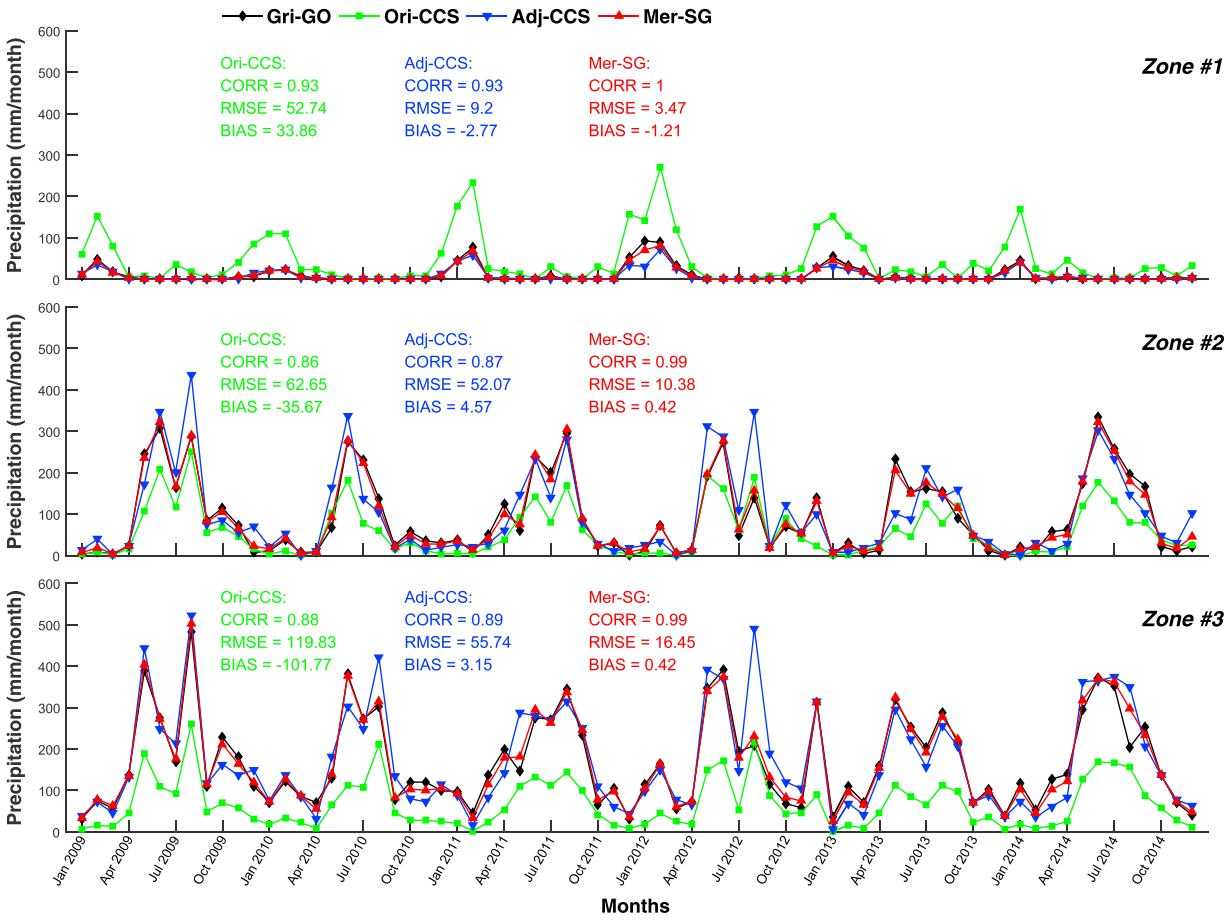

Figure 9. Monthly areal mean precipitation series of Gri-GO, Ori-CCS, Adj-CCS, and Mer-SG over the evaluation zones during 2009–2014.

The merged monthly precipitation series exhibit high data quality after blending the Gri-GO and Adj-CCS estimates. As shown in Figure 9, the monthly estimates of Mer-SG present further improved consistency with the reference data over all zones compared to that of Adj-CCS. In particular, the random errors observed in Adj-CCS estimations have been significantly reduced after data merging for those specific months (e.g., August 2012). As a result, the CORRs for Mer-SG increase to a value close to 1.0, while the RMSEs are reduced to a range between 3.47 and 16.45 mm/month and the absolute BIASs show low values between −1.21 and 0.42 mm/month. These improvements are due to incorporating simultaneous gauge observations into the systematic bias-adjusted satellite precipitation estimates.

4.1.2.2. Daily

The daily areal mean precipitation series from calibration are shown in scatterplots for the period of 2009–2014 (Figure 10). Corresponding PODs, FARs, and HSSs for the Ori-CC, Adj-CCS, and Mer-SG daily estimates are calculated and presented in Table 1. According to Figure 10, the daily precipitation was overestimated by Ori-CCS over zone no. 1 and underestimated over zone nos. 2 and 3. For Adj-CCS, systematic biases in the daily precipitation series are removed effectively, as indicated by the great decreases in the absolute BIAS (to less than 0.1 mm/d). However, the other indicators for Adj-CCS including CORR, RMSE, POD, FAR, and HSS do not exhibit significant improvements for zone nos. 2 and 3. Similar results were also found in *Yang et al.* [2016].

After data merging, great improvement has been observed for the daily estimates, as shown by the high consistency of Mer-SG with Gri-GO estimates for all zones, with the values clustering around the 1:1 lines in Figure 10. In consequence, the RMSEs for Mer-SG over all zones are greatly decreased to 0.27–2.69 mm/d and the CORRs reach to over 0.95; all the PODs and HSSs are improved to 1.00 and over 0.65, respectively, with decreased FARs (Table 1).

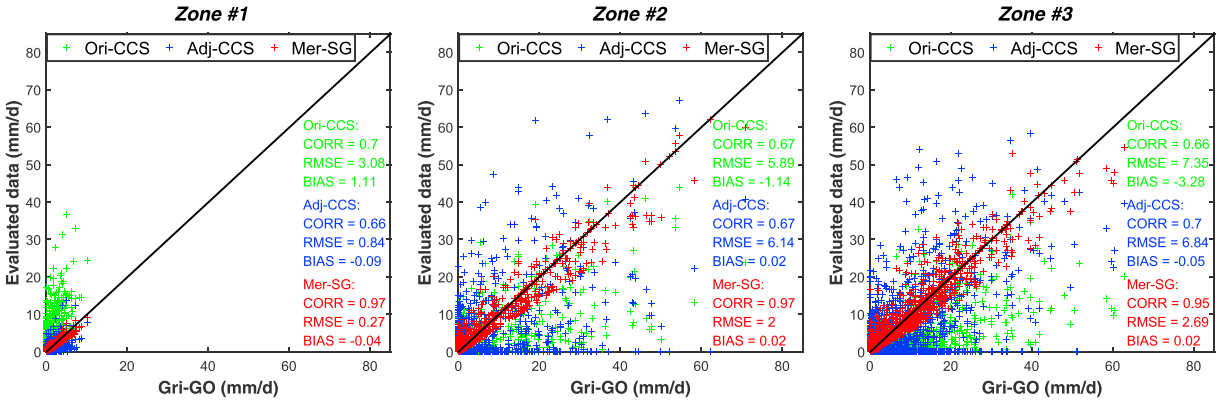

Figure 10. Scatterplots of daily areal mean precipitation series for Ori-CCS, Adj-CCS, and Mer-SG against Gri-GO estimates over the evaluation zones during 2009–2014.

4.2. Validation Results

4.2.1. Monthly Estimates

The monthly average precipitation time series for the gauge observation, Ori-CCS, Adj-CCS, and Mer-SG are presented for the validation gauge groups (Figure 4b) during 2009–2014 (Figure 11). From Figure 11, the Ori-CCS shows overestimated monthly precipitation over group nos. 1 and 2 and exhibits large underestimations over group no. 3, resulting in high RMSEs and BIASs. After systematic bias adjustment, the monthly estimates for Adj-CCS are improved with great decreases in absolute BIAS and RMSE by on average 90% and 53%, respectively. Nonetheless, some high random errors still remain in the Adj-CCS monthly estimates leading to RMSEs of up to 47.36 mm/month and almost unchanged CORRs, showing a similar pattern to the monthly results from the calibration phase.

After incorporating simultaneous ground observations, the data merging framework has provided a good quality monthly precipitation time series over the validation groups (Figure 11). As shown in Figure 11, the Mer-SG monthly estimates have been effectively shifted toward the reference observations, especially for those high precipitation months with large random errors observed in Adj-CCS (e.g., August 2012). These changes cause the CORRs for Mer-SG to exceed 0.98 and bring the RMSEs down to 2.61 ~ 12.41 mm/month, with insignificant BIAS values remaining after data merging.

4.2.2. Daily Estimates

As shown in Figure 12, the daily average precipitation series for Ori-CCS (green "plus sign"), Adj-CCS (blue "plus sign"), and Mer-SG (red "plus sign") are assessed over the validation groups as well. Figure 13 and Table 2 present the corresponding CDFs, PODs, FARs, and HSSs calculated for these precipitation estimates. From Figure 12, the Ori-CCS tends to overestimate daily precipitation over group nos. 1 and 2 and to underestimate over group no. 3, leading to relatively low CORRs and high RMSEs and absolute BIASs. For Adj-CCS, improvements have been spotted for the daily estimates over the validation groups, exhibiting great reductions of absolute BIASs to less than 0.1 mm/d after removing the systematic biases in the Ori-CCS precipitation estimates. The systematic bias reductions are evidenced by the consistently improved CDFs of Adj-CCS

Table 1. PODs, FARs, and HSSs of Daily Precipitation Estimates From Calibration

Evaluation Zone	Statistic	Ori-CCS	Adj-CCS	Mer-SG
Zone no. 1	POD	0.88	0.81	1.00
	FAR	0.45	0.37	0.33
	HSS	0.39	0.49	0.65
Zone no. 2	POD	0.66	0.65	1.00
	FAR	0.10	0.10	0.06
	HSS	0.16	0.16	0.76
Zone no. 3	POD	0.75	0.75	1.00
	FAR	0.03	0.03	0.02
	HSS	0.32	0.32	0.67

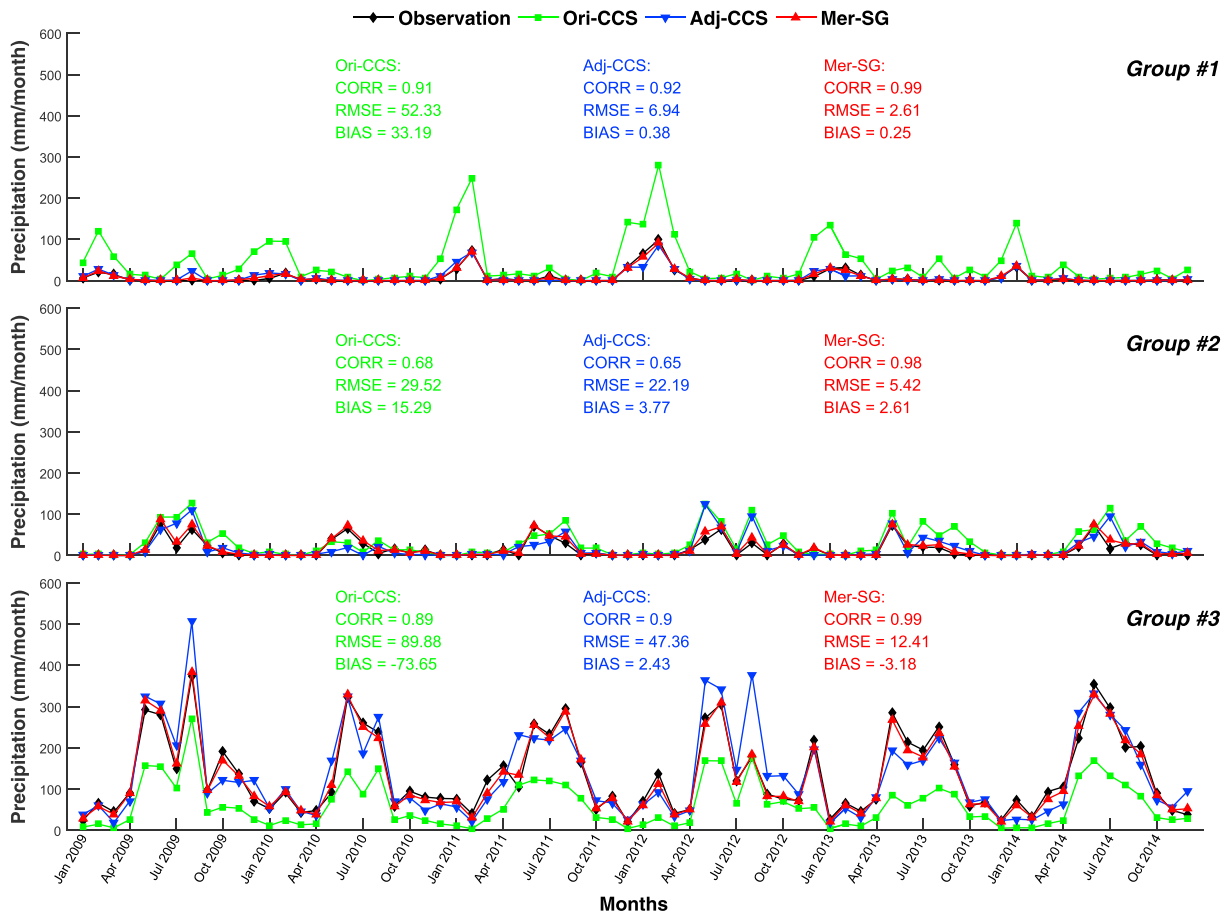

Figure 11. Monthly average precipitation series of gauge observation, Ori-CCS, Adj-CCS, and Mer-SG over the validation gauge groups during 2009–2014.

compared to Ori-CCS over all groups, as evaluated using the corresponding CDFs of gauge observed data (see Figure 13). However, no significant improvements in the CORRs, RMSEs, PODs, FARs, and HSSs for Adj-CCS are shown, especially for group nos. 2 and 3 (Figure 12 and Table 2).

These precipitation errors in the validation groups are brought down via the merging of gauge and satellite estimates. As presented in Figure 12, the Mer-SG daily estimates show high consistency with the gauge measurements, with values clustering around the 1:1 lines for all groups. The CORRs for Mer-SG in consequence increase to 0.94 and the RMSEs decrease to 1.04 mm/d, on average. In addition, the CDFs for Mer-SG estimates fit well with those for gauge observations across the validation groups (Figure 13). These results indicate good performance of the merged precipitation data over the 42 evaluated pixels/gauges, suggesting effectiveness of the framework in producing accurate precipitation data even over ungauged spatial coverage areas. However, the Mer-SG daily estimates show common increases in FARs and decreases in HSSs over the groups, while the PODs are improved to 0.93–1.00, when compared to those for the Adj-CCS series (Table 2). These FAR increases are coincident with the underestimated CDF values for Mer-SG estimates over those nonrainy days (see Figure 13).

To evaluate the differences between the statistics for these SPE products, the number of rainy days (NRD), RMSE, and BIAS for each Ori-CCS, Adj-CCS, and Mer-SG daily series are examined with respect to different rainfall amount ranges over the validation gauge groups. As shown in Figure 14, Ori-CCS presents the highest NRDs for those nonrainy days (indicating false alarms) over group nos. 1 and 2, located in the dry areas of north and central Chile. Group no. 3 (located in the wet south) shows high disagreement between the NRDs for Ori-CCS and ground-based observations especially for rainy days with a precipitation amount of less-than 10 mm/d. After systematic bias correction, the NRDs for Adj-CCS are commonly reduced over group nos. 1 and 2, particularly for the nonrainy days, and group no. 3 exhibits relatively stable NRDs across all

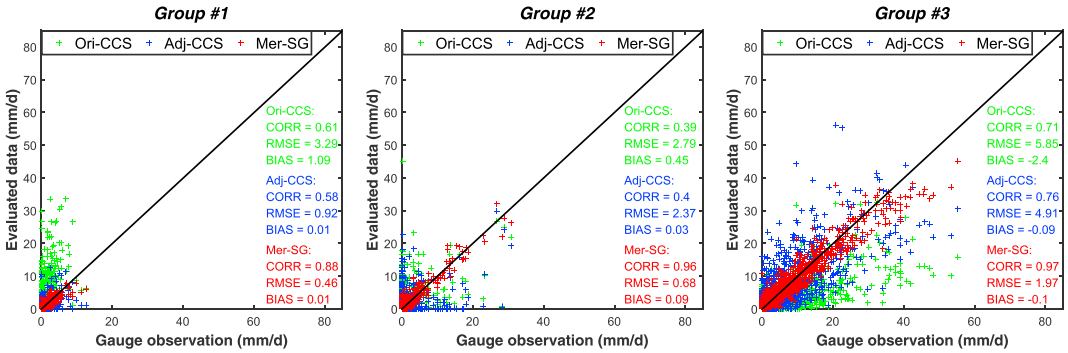

Figure 12. Scatterplots of daily average precipitation series of Ori-CCS, Adj-CCS, and Mer-SG against gauge observations over the validation gauge groups during 2009–2014.

rainfall amount ranges. These changes can account for the FAR and POD decreases and slight HSS increases for Adj-CCS over group nos. 1 and 2, as well as the minor changes in FAR, POD, and HSS over group no. 3 (see Table 2). In contrast, Mer-SG shows greatly improved NRDs for rainy days (rainfall amount $>$ 0 mm/d) compared to observations, due to incorporating the gridded gauge data that helps to fix the misses from the SPE. This improvement has caused the increased PODs for Mer-SG as shown in Table 2. On the other hand, a higher NRD is observed in the case of the Mer-SG for the nonrainy days (Figure 14), which can be interpreted from the CDFs for Mer-SG (see Figure 13). It helps to explain the FAR increases for Mer-SG and the consequently deteriorated HSSs over the validation groups (Table 2). The main reason for the aggravated NRDs and FARs for Mer-SG might be the incorporation of FARs from Gri-GO estimates generated from the gauge observation gridding procedure that could be too coarse for zero-rainfall detection.

In addition, the RMSE and BIAS for Ori-CCS (green lines) generally increase as observed rainfall amount rises (Figure 14). Due to systematic bias adjustment, the Adj-CCS (blue lines) presents consistent reductions of

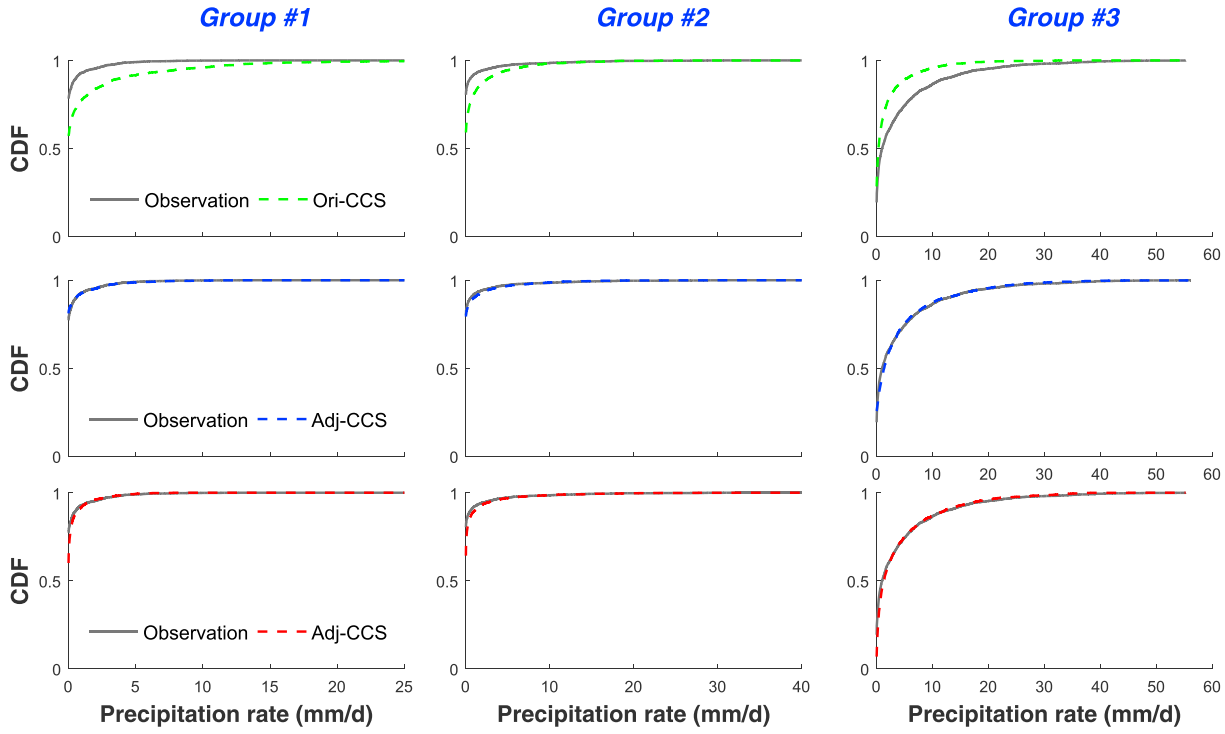

Figure 13. Comparison of CDFs calculated for gauge observation (grey solid line), Ori-CCS (green dash line), Adj-CCS (blue dash line), and Mer-SG (red dash line) over the validation groups.

Table 2. PODs, FARs, and HSSs of Daily Precipitation Estimates From Validation

Evaluation Group	Statistic	Ori-CCS	Adj-CCS	Mer-SG
Group no. 1	POD	0.83	0.58	0.93
	FAR	0.56	0.32	0.51
	HSS	0.39	0.52	0.48
Group no. 2	POD	0.69	0.45	0.98
	FAR	0.62	0.56	0.63
	HSS	0.26	0.27	0.29
Group no. 3	POD	0.82	0.81	1.00
	FAR	0.09	0.08	0.12
	HSS	0.31	0.31	0.17

RMSE and BIAS over group no. 1 (throughout the rainfall rate ranges) and group no. 3 (mainly for heavy precipitation), with the statistics for group no. 2 remaining almost unchanged. The merged precipitation estimates (red lines) show further decreased RMSEs and BIASs, especially for validation group nos. 2 and 3 (Figure 14). It indicates greatly improved precision of the Mer-SG precipitation estimates over the areas without gauge observations. Furthermore, the false alarms from Mer-SG (observed rainfall amount = 0 mm/d; see Figure 14) have resulted in limited RMSEs and BIASs because the overestimated rainfall rates are low, as can be seen from the CDFs of Mer-SG and gauge observation (Figure 13). This implies that false alarm-induced uncertainties in the merged precipitation data can be neglected, especially when these data are used for hydrologic applications.

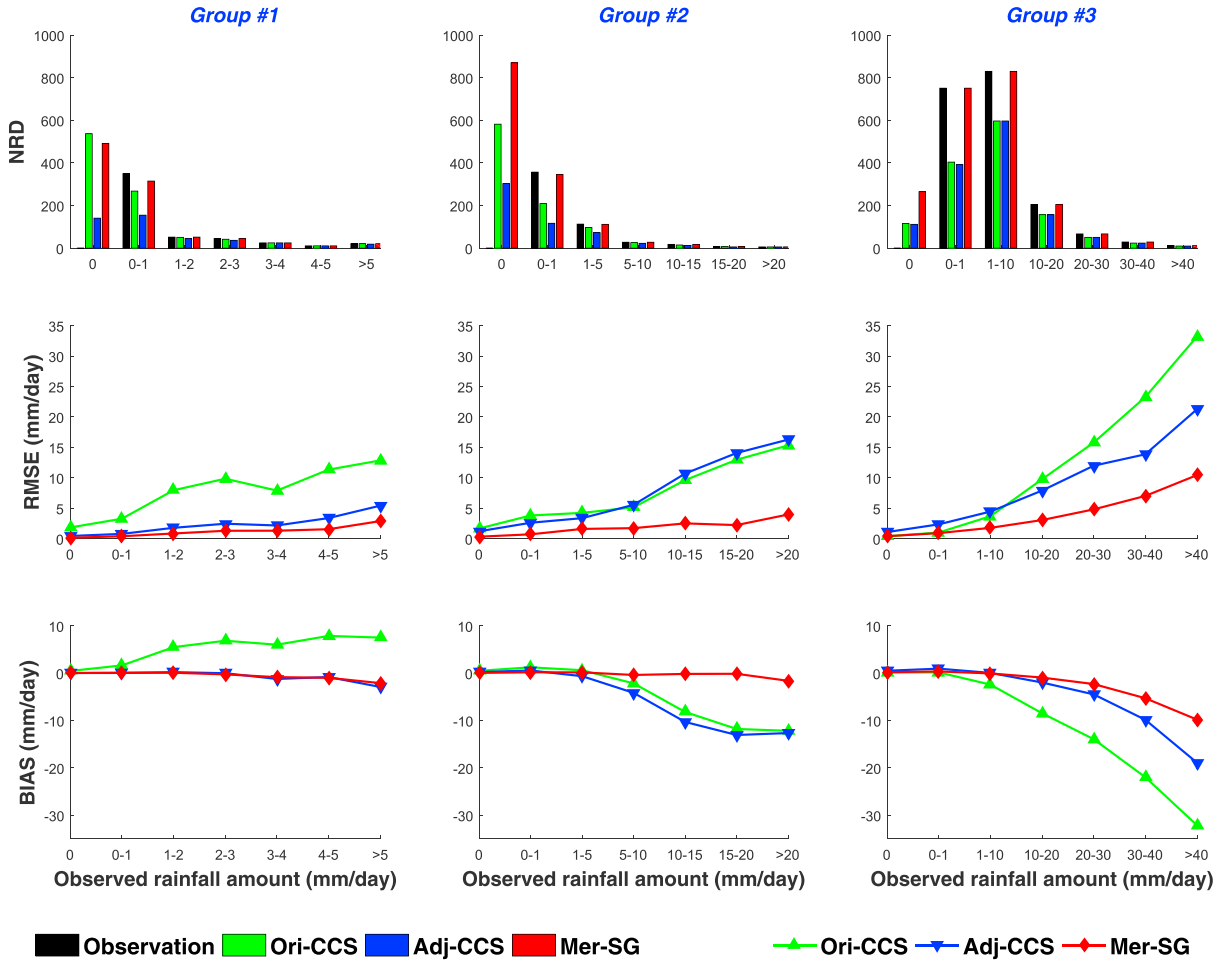

Figure 14. The (top) NRDs, (middle) RMSEs, and (bottom) BIASs of Ori-CCS, Adj-CCS, and Mer-SG daily precipitation averages over the validation gauge groups for different observed rainfall amount ranges during 2009–2014.

5. Conclusions and Future Prospects

This study provided a framework for merging satellite-based precipitation field estimation and point-scale gauge observation with three separate steps. A case study over Chile was conducted to verify the effectiveness of the model using PERSIANN-CCS daily precipitation estimates and corresponding gauge data during 2009–2014. According to the findings, the following conclusions can be drawn: (1) The framework is effective in producing satellite-gauge merged precipitation data with high resolution and precision. The bias adjustment step helps to remove systematic biases in satellite data, and the data merging step further improves the precipitation estimation accuracy, indicated by very high CORRs and significantly reduced RMSEs and absolute BIASs from evaluation. (2) The model validation confirms that the framework is able to greatly improve the POD and accuracy of generated precipitation estimates even over those areas where gauge data are absent.

Therefore, this study serves as a valuable pilot case for precipitation data merging in view of its further application over different areas worldwide. Two recommendations are made for its future applications. First, care should be taken in model calibration. The gauge data gridding parameter (C) and weighting functions (f(DMIN)) of the model can directly impact the spatial pattern and accuracy of merged precipitation estimates, as they need to be determined and fitted in advance. Especially when the model is applied to a large-scale territory, RMSE functions for suitable regional coverage should be considered in the data merging process. Therefore, attention should be paid to the parameter sensitivities and advanced parameterization approaches for spatially variable uncertainty quantification in future applications. Second, while in this study historical data sets are used covering the period of 2009–2014 for calibrating the model for satellite-gauge data merging, a next step would be to apply the framework to generate near real-time precipitation products. In this study, the satellite-gauge data merging is conducted under an assumption that biases of each data set are "systematic" or stationary across 2009–2014. How the calibrated model performs outside the 2009–2014 period needs further investigation in future near-real-time data merging. By providing merged near-real-time SPE, additional gains can be made to provide relevant databases for hydrologic and climatic applications for decision making, especially over the areas where gauged hydroclimatic records are limited in both spatial and temporal coverage [*Kidd et al.*, 2017; *Kiem et al.*, 2016; *Liu et al.*, 2017].

Acknowledgments

This study is sponsored by the National Technology Support Program Funds for the Key Technology for Digital Basin (project 2013BAB05B04) and by the China Scholarship Council (201406040177). The constructive comments and suggestions by the journal referees are gratefully acknowledged. The daily rain gauge observations and PERSIANN-CCS precipitation estimates used in this study are available at http://www.climatedatalibrary.cl/SOURCES/.Chile/.DGA/.meteorological/.Precipitation/.Historical/.Daily/ and http://chrs.web.uci.edu/, respectively.

References

Adler, R. F., et al. (2003), The version-2 global precipitation climatology project (GPCP) monthly precipitation analysis (1979–Present), *J. Hydrometeorol.*, *4*(6), 1147–1167, doi:10.1175/1525-7541(2003)004<1147:tvgpcp>2.0.co;2.

AghaKouchak, A., A. Behrangi, S. Sorooshian, K. Hsu, and E. Amitai (2011), Evaluation of satellite-retrieved extreme precipitation rates across the central United States, *J. Geophys. Res.*, *116*, D02115, doi:10.1029/2010JD014741.

Ashouri, H., K. Hsu, S. Sorooshian, D. K. Braithwaite, K. R. Knapp, L. D. Cecil, B. R. Nelson, and O. P. Prat (2015), PERSIANN-CDR: Daily precipitation climate data record from multisatellite observations for hydrological and climate studies, *Bull. Am. Meteorol. Soc.*, *96*(1), 69–83, doi:10.1175/bams-d-13-00068.1.

Beck, H. E., A. I. J. M. van Dijk, V. Levizzani, J. Schellekens, D. G. Miralles, B. Martens, and A. de Roo (2016), MSWEP: 3-hourly 0.25° global gridded precipitation (1979–2015) by merging gauge, satellite, and reanalysis data, *Hydrol. Earth Syst. Sci. Discuss.*, *2016*, 1–38, doi:10.5194/hess-2016-236.

Behrangi, A., K. Andreadis, J. B. Fisher, F. J. Turk, S. Granger, T. Painter, and N. Das (2014), Satellite-based precipitation estimation and its application for streamflow prediction over mountainous western US basins, *J. Appl. Meteorol. Climatol.*, *53*(12), 2823–2842, doi:10.1175/jamc-d-14-0056.1.

Bitew, M. M., and M. Gebremichael (2011), Evaluation of satellite rainfall products through hydrologic simulation in a fully distributed hydrologic model, *Water Resour. Res.*, *47*, W06526, doi:10.1029/2010WR009917.

Chaney, N. W., J. Sheffield, G. Villarini, and E. F. Wood (2014), Development of a high-resolution gridded daily meteorological dataset over sub-Saharan Africa: Spatial analysis of trends in climate extremes, *J. Clim.*, *27*(15), 5815–5835, doi:10.1175/JCLI-D-13-00423.1.

Chubb, T. H., M. J. Manton, S. T. Siems, and A. D. Peace (2016), Evaluation of the AWAP daily precipitation spatial analysis with an independent gauge network in the Snowy Mountains, *J. South. Hemisphere Earth Syst. Sci.*, *66*(1), 55–67.

De Vera, A., and R. Terra (2012), Combining CMORPH and rain gauges observations over the Rio Negro Basin, *J. Hydrometeorol.*, *13*(6), 1799–1809, doi:10.1175/jhm-d-12-010.1.

Funk, C., et al. (2015), The climate hazards infrared precipitation with stations—A new environmental record for monitoring extremes, *Sci. Data*, *2*, 150066, doi:10.1038/sdata.2015.66.

Gebregiorgis, A. S., Y. D. Tian, C. D. Peters-Lidard, and F. Hossain (2012), Tracing hydrologic model simulation error as a function of satellite rainfall estimation bias components and land use and land cover conditions, *Water Resour. Res.*, *48*, W11509, doi:10.1029/2011WR011643.

Hong, Y., K. Hsu, S. Sorooshian, and X. Gao (2004), Precipitation estimation from remotely sensed imagery using an artificial neural network cloud classification system, *J. Appl. Meteorol.*, *43*(12), 1834–1852, doi:10.1175/jam2173.1.

Hsu, K., X. Gao, S. Sorooshian, and H. V. Gupta (1997), Precipitation estimation from remotely sensed information using artificial neural networks, *J. Appl. Meteorol.*, *36*(9), 1176–1190.

Hsu, K., H. V. Gupta, X. Gao, and S. Sorooshian (1999), Estimation of physical variables from multichannel remotely sensed imagery using a neural network: Application to rainfall estimation, *Water Resour. Res.*, *35*, 1605–1618.

Huff, F. (1970), Sampling errors in measurement of mean precipitation, *J. Appl. Meteorol.*, *9*(1), 35–44.

Huffman, G. J., R. F. Adler, P. Arkin, A. Chang, R. Ferraro, A. Gruber, J. Janowiak, A. McNab, B. Rudolf, and U. Schneider (1997), The Global Precipitation Climatology Project (GPCP) combined precipitation dataset, *Bull. Am. Meteorol. Soc.*, *78*(1), 5–20, doi:10.1175/1520-0477(1997)078<0005:tgpcpg>2.0.co;2.

Huffman, G. J., R. F. Adler, D. T. Bolvin, and E. J. Nelkin (2010), *The TRMM Multi-Satellite Precipitation Analysis (TMPA)*, pp. 3–22, Springer, Netherlands, doi:10.1007/978-90-481-2915-7_1.

Huffman, G. J., D. T. Bolvin, E. J. Nelkin, D. B. Wolff, R. F. Adler, G. Gu, Y. Hong, K. P. Bowman, and E. F. Stocker (2007), The TRMM multisatellite precipitation analysis (TMPA): Quasi-global, multiyear, combined-sensor precipitation estimates at fine scales, *J. Hydrometeorol.*, *8*(1), 38–55, doi:10.1175/JHM560.1.

Huffman, G. J., D. T. Bolvin, D. Braithwaite, K. Hsu, R. Joyce, and P. Xie (2014), GPM Integrated Multi-Satellite Retrievals for GPM (IMERG) Algorithm Theoretical Basis Document (ATBD) version 4.4. Rep.

Hyvarinen, O. (2014), A probabilistic derivation of Heidke skill score, *Weather Forecasting*, *29*(1), 177–181.

Joyce, R. J., J. E. Janowiak, P. A. Arkin, and P. Xie (2004), CMORPH: A method that produces global precipitation estimates from passive microwave and infrared data at high spatial and temporal resolution, *J. Hydrometeorol.*, *5*(3), 487–503.

Kidd, C., A. Becker, G. J. Huffman, C. L. Muller, P. Joe, G. Skofronick-Jackson, and D. B. Kirschbaum (2017), So, how much of the Earth's surface is covered by rain gauges?, *Bull. Am. Meteorol. Soc.*, *98*(1), 69–78, doi:10.1175/bams-d-14-00283.1.

Kiem, A. S., et al. (2016), Natural hazards in Australia: Droughts, *Clim. Change*, *139*(1), 37–54, doi:10.1007/s10584-016-1798-7.

King, A. D., L. V. Alexander, and M. G. Donat (2013), The efficacy of using gridded data to examine extreme rainfall characteristics: A case study for Australia, *Int. J. Climatol.*, *33*(10), 2376–2387, doi:10.1002/joc.3588.

Kubota, T., et al. (2007), Global precipitation map using satellite-borne microwave radiometers by the GSMaP project: Production and validation, *IEEE Trans. Geosci. Remote Sens.*, *45*(7), 2259–2275, doi:10.1109/tgrs.2007.895337.

Li, M., and Q. Shao (2010), An improved statistical approach to merge satellite rainfall estimates and raingauge data, *J. Hydrol.*, *385*, 51–64, doi:10.1016/j.jhydrol.2010.01.023.

Li, Z., D. W. Yang, and Y. Hong (2013), Multi-scale evaluation of high-resolution multi-sensor blended global precipitation products over the Yangtze River, *J. Hydrol.*, *500*, 157–169, doi:10.1016/j.jhydrol.2013.07.023.

Liu, H., S. Sorooshian, and X. G. Gao (2015), Assessment of the spatial and seasonal variation of the error-intensity relationship in satellite-based precipitation measurements using an adaptive parametric model, *J. Hydrometeorol.*, *16*(4), 1700–1716, doi:10.1175/jhm-d-14-0219.1.

Liu, X., T. Yang, K. Hsu, C. Liu, and S. Sorooshian (2017), Evaluating the streamflow simulation capability of PERSIANN-CDR daily rainfall products in two river basins on the Tibetan Plateau, *Hydrol. Earth Syst. Sci.*, *21*(1), 169–181, doi:10.5194/hess-21-169-2017.

Melo, D. D. D., A. C. Xavier, T. Bianchi, P. T. S. Oliveira, B. R. Scanlon, M. C. Lucas, and E. Wendland (2015), Performance evaluation of rainfall estimates by TRMM Multi-satellite Precipitation Analysis 3B42V6 and V7 over Brazil, *J. Geophys. Res. Atmos.*, *120*, 9426–9436, doi:10.1002/2015JD023797.

Miao, C., H. Ashouri, K. L. Hsu, S. Sorooshian, and Q. Y. Duan (2015), Evaluation of the PERSIANN-CDR daily rainfall estimates in capturing the behavior of extreme precipitation events over China, *J. Hydrometeorol.*, *16*(3), 1387–1396, doi:10.1175/jhm-d-14-0174.1.

Miao, C., L. Su, Q. Sun, and Q. Duan (2016a), A nonstationary bias-correction technique to remove bias in GCM simulations, *J. Geophys. Res. Atmos.*, *121*, 5718–5735, doi:10.1002/2015JD024159.

Miao, C., Q. Sun, Q. Duan, and Y. Wang (2016b), Joint analysis of changes in temperature and precipitation on the loess plateau during the period 1961–2011, *Clim. Dyn.*, *47*(9–10), 3221–3234, doi:10.1007/s00382-016-3022-x.

Mitchell, K. E., D. Lohmann, P. R. Houser, E. F. Wood, J. C. Schaake, A. Robock, B. A. Cosgrove, J. Sheffield, Q. Duan, and L. Luo (2004), The multi-institution North American Land Data Assimilation System (NLDAS): Utilizing multiple GCIP products and partners in a continental distributed hydrological modeling system, *J. Geophys. Res.*, *109*, D07S90, doi:10.1029/2003JD003823.

Moradkhani, H., and S. Sorooshian (2008), General review of rainfall-runoff modeling: Model calibration, data Assimilation, and uncertainty analysis, in *Hydrological Modelling and the Water Cycle: Coupling the Atmosheric and Hydrological Models*, edited by S. Sorooshian et al., pp. 1–24, Springer, Berlin.

Peng, L., J. Sheffield, and K. Verbist (2016), Merging station observations with large-scale gridded data to improve hydrological predictions 20 over Chile, in AGU Fall Meeting Abstract, San Francisco, Calif.

Sarachi, S., K. Hsu, and S. Sorooshian (2015), A statistical model for the uncertainty analysis of satellite precipitation products, *J. Hydrometeorol.*, *16*(5), 2101–2117, doi:10.1175/JHM-D-15-0028.1.

Satge, F., M. P. Bonnet, M. Gosset, J. Molina, W. H. Y. Lima, R. P. Zola, F. Timouk, and J. Garnier (2016), Assessment of satellite rainfall products over the Andean plateau, *Atmos. Res.*, *167*, 1–14, doi:10.1016/j.atmosres.2015.07.012.

Sorooshian, S., K. Hsu, X. Gao, H. V. Gupta, B. Imam, and D. Braithwaite (2000), Evaluation of PERSIANN system satellite-based estimates of tropical rainfall, *Bull. Am. Meteorol. Soc.*, *81*(9), 2035–2046, doi:10.1175/1520-0477(2000)081<2035:eopsse>2.3.co;2.

Su, F., H. Gao, G. J. Huffman, and D. P. Lettenmaier (2011), Potential utility of the real-time TMPA-RT precipitation estimates in streamflow prediction, *J. Hydrometeorol.*, *12*(3), 444–455, doi:10.1175/2010JHM1353.1.

Themessl, M. J., A. Gobiet, and G. Heinrich (2012), Empirical-statistical downscaling and error correction of regional climate models and its impact on the climate change signal, *Clim. Chang.*, *112*(2), 449–468, doi:10.1007/s10584-011-0224-4.

Thiemig, V., R. Rojas, M. Zambrano-Bigiarini, and A. De Roo (2013), Hydrological evaluation of satellite-based rainfall estimates over the Volta and Baro-Akobo Basin, *J. Hydrol.*, *499*, 324–338, doi:10.1016/j.jhydrol.2013.07.012.

Tian, Y., C. D. Peters-Lidard, J. B. Eylander, R. J. Joyce, G. J. Huffman, R. F. Adler, K. Hsu, F. J. Turk, M. Garcia, and J. Zeng (2009), Component analysis of errors in satellite-based precipitation estimates, *J. Geophys. Res.*, *114*, D24101, doi:10.1029/2009JD011949.

Tozer, C. R., A. S. Kiem, and D. C. Verdon-Kidd (2012), On the uncertainties associated with using gridded rainfall data as a proxy for observed, *Hydrol. Earth Syst. Sci.*, *16*(5), 1481–1499, doi:10.5194/hess-16-1481-2012.

Vila, D. A., L. G. G. de Goncalves, D. L. Toll, and J. R. Rozante (2009), Statistical evaluation of combined daily gauge observations and rainfall satellite estimates over continental South America, *J. Hydrometeorol.*, *10*(2), 533–543, doi:10.1175/2008jhm1048.1.

Xie, P., and A.-Y. Xiong (2011), A conceptual model for constructing high-resolution gauge-satellite merged precipitation analyses, *J. Geophys. Res.*, *116*, D21106, doi:10.1029/2011JD016118.

Yang, T., A. Akbari Asanjan, E. Welles, X. Gao, S. Sorooshian, and X. Liu (2017), Developing reservoir monthly inflow forecasts using artificial intelligence and climate phenomenon information, *Water Resour. Res.*, doi:10.1002/2017WR020482.

Yang, Z., K. Hsu, S. Sorooshian, X. Xu, D. Braithwaite, and K. M. J. Verbist (2016), Bias adjustment of satellite-based precipitation estimation using gauge observations: A case study in Chile, *J. Geophys. Res. Atmos.*, *121*, 3790–3806, doi:10.1002/2015JD024540.

Zambrano-Bigiarini, M., A. Nauditt, C. Birkel, K. Verbist, and L. Ribbe (2017), Temporal and spatial evaluation of satellite-based rainfall estimates across the complex topographical and climatic gradients of Chile, *Hydrol. Earth Syst. Sci.*, *21*(2), 1295–1320, doi:10.5194/hess-21-1295-2017.